Contents lists available at ScienceDirect

# Deep-Sea Research II

journal homepage: www.elsevier.com/locate/dsr2

# Initial results of comparing cold-seep carbonates from mussel- and tubeworm-associated environments at Atwater Valley lease block 340, northern Gulf of Mexico

Dong Feng [a,b], Harry H. Roberts [b,*]

[a] CAS Key Laboratory of Marginal Sea Geology, Guangzhou Institute of Geochemistry, Chinese Academy of Sciences, Guangzhou 510640, China
[b] Coastal Studies Institute, Department of Oceanography and Coastal Sciences, Louisiana State University, Baton Rouge, LA 70803, USA

## ARTICLE INFO

## ABSTRACT

Chemosymbiotic macrofauna (such as mussels and tubeworms) and authigenic carbonates are typical of many hydrocarbon seeps. To address whether mussels and tubeworms could impact the sediment geochemistry of their habitat where authigenic carbonates are precipitated, a comparative study of petrographic and geochemical features of the authigenic carbonates from mussel- and tubeworm-associated environments at hydrocarbon seeps in Atwater Valley lease area block 340 (AT340) of the Gulf of Mexico was undertaken. Both mussel- and tubeworm-associated carbonates are dominated by high-magnesium calcite (HMC) and aragonite, and two tubeworm-associated carbonate samples have minor amounts of dolomite. The $\delta^{13}C$ values of all carbonates are low, ranging from $-60.8‰$ to $-35.5‰$ PDB. Although there is much overlap, surprisingly the $\delta^{13}C$ values of mussel-associated carbonates are generally higher than those of tubeworm-associated carbonates ($-51.8‰$ vs. $-54.8‰$ for an average of over 60 subsamples). It is suggested that (1) carbon isotopic vital effect of seep mussels and tubeworms, (2) fluid physical pumping of mussels, and (3) release of sulfate by tubeworm roots may be responsible for the relatively lower $\delta^{13}C$ values of tubeworm-associated carbonates. It has been suggested that the heterogeneities in mineralogy and stable carbon isotope geochemistry of the seep carbonates may be attributed to the activity of macrofauna (mussels and tubeworms) and associated microbes. Our observations also suggest that at AT340 the geochemical evolution of seep macrofauna is from a mussel-dominated environment to a mixed mussel-tubeworm environment, and finally to a mostly tubeworm-dominated environment. This evolution is controlled mainly by the habitat, e.g., hydrocarbon seep flux.

## 1. Introduction

Many of the world's productive deepwater hydrocarbon basins experience significant and ongoing vertical migration of hydrocarbons to the modern seafloor (e.g., Roberts and Aharon, 1994; Peckmann and Thiel, 2004; Campbell, 2006; Roberts et al., 2007a; Cordes et al., 2009). The geological and biological impacts of hydrocarbon seepage on the seafloor are related to the composition of products being delivered to the seafloor, the delivery rates of these products, and the history of fluid-gas migration seepage at a given site (Roberts et al., 1990; Roberts and Carney, 1997; Roberts, 2001; Feng et al., 2009). Methane arriving at the seafloor can be biogenic or thermogenic in origin, or a combination of both (Roberts and Aharon, 1994; Peckmann and Thiel, 2004; Naehr et al., 2007). Qualitative delivery rates range from slow to rapid. Biological and

geological responses at the seafloor are significantly different when affected by sustained and different delivery rates of hydrocarbon seepage (Roberts and Carney, 1997; Roberts, 2001; Feng et al., 2009). When delivery products and rates are compatible with a physically stable seafloor and provide the appropriate trophic resources for chemoautotrophy and methanotrophy, densely populated and diverse animal communities may arise. The composition of these communities can change as the nature of the seepage evolves.

Authigenic carbonate, a by-product of seeping hydrocarbons, is usually promoted by relatively slow seepage (Roberts and Carney, 1997; Roberts, 2001; Luff and Wallmann, 2003). It is now well established that carbonate precipitation at hydrocarbon seeps is closely related to the Anaerobic Oxidation of Methane (AOM) (Boetius et al., 2000), or higher molecular-weight hydrocarbons (Formolo et al., 2004; Joye et al., 2004). The process is microbially mediated and occurs under anoxic conditions where methane oxidation is coupled to sulfate reduction, resulting in overall production of bicarbonate that is ultimately precipitated as authigenic carbonate. The microorganisms responsible for AOM are generally thought to comprise

---

* Corresponding author. Tel.: +1 225 578 2395; fax: +1 225 578 2520.
E-mail addresses: dongfeng@lsu.edu (D. Feng), hrober3@lsu.edu (H.H. Roberts).

consortia of methane-consuming archaea and sulfate-reducing bacteria (e.g., Hinrichs et al., 1999; Boetius et al., 2000). Chemosynthesis suggests that macrofauna such as mussels and tubeworms are abundant at many hydrocarbon seeps (see Cordes et al., 2009, and Levin, 2005, and references therein). These aggregations in theory could exert a significant impact on the geochemistry of the surrounding rhizosphere (Cordes et al., 2003, 2005; Dattagupta et al., 2006, 2008). However, questions remain about the modification of sedimentary geochemistry by hydrocarbon seep mussels and tubeworms. The evolution (e.g., diversity and variability) of seep macrofauna over time-scales is also not clear.

The fundamental question addressed in our research relates to whether differences in the geochemical environment of mussels and tubeworms are sufficient to influence associated authigenic carbonates. To address whether mussels and tubeworms impact the geology and geochemistry of their habitat where authigenic carbonates are precipitated, petrographic and geochemical analyses of the carbonate from mussel- and tubeworm-associated environments were conducted. These observations were then used to suggest a simple schematic model showing the evolution of seep macrofauna at hydrocarbon seeps.

## 2. Site characteristics and sampling

During 2006 and 2007, Deep Submergence Vehicle (DSV) ALVIN and Remotely Operated Vehicle (ROV) JASON were used to conduct sampling at Atwater Valley lease area block 340 (AT340), located in approximately 2200 m water depth on the lower Louisiana slope of the Gulf of Mexico (GOM). The AT340 dive site is geologically characterized as a bathymetric high along the eastern extension of the Mississippi Canyon where it transitions from a canyon to an unconfined submarine fan (Fig. 1). The site consists of three localized mounded areas on top of the overall bathymetric high (Fig. 2). Geophysical data indicate that the feature is supported by salt in the shallow subsurface. Seismic profiles identify a clear vertical migration pathway from the deep subsurface to the ocean bottom. This pathway is defined by acoustic blanking of the seismic records, suggesting both scattering of acoustic energy, by gas perhaps, and hard-bottom conditions at the surface. The surface reflectivity maps, created by analyzing the first return of the sediment-water interface from 3D seismic data, indicate high reflectivity associated with localized mounded features.

On the 3D seismic surface reflectivity maps, the southeast quadrant of the AT340 study area displayed a complex pattern of high to moderate reflectivity. Observations from DSV ALVIN and ROV JASON confirmed extensive hard-bottom conditions that resulted from the presence of massive carbonates. Inspection of these carbonates revealed that they commonly contained abundant mussel shells. In addition, abundant carbonates were observed around the bases of tubeworm bushes. Living tubeworm colonies and mussel beds were scattered throughout the authigenic carbonate blocks and pavements (Fig. 3A). Lessard-Pilon et al. (2010) addressed the community composition and temporal change of our sample site. High surface reflectivity in the northwestern part of the study area was found to be associated with a mound of carbonate blocks composed mostly
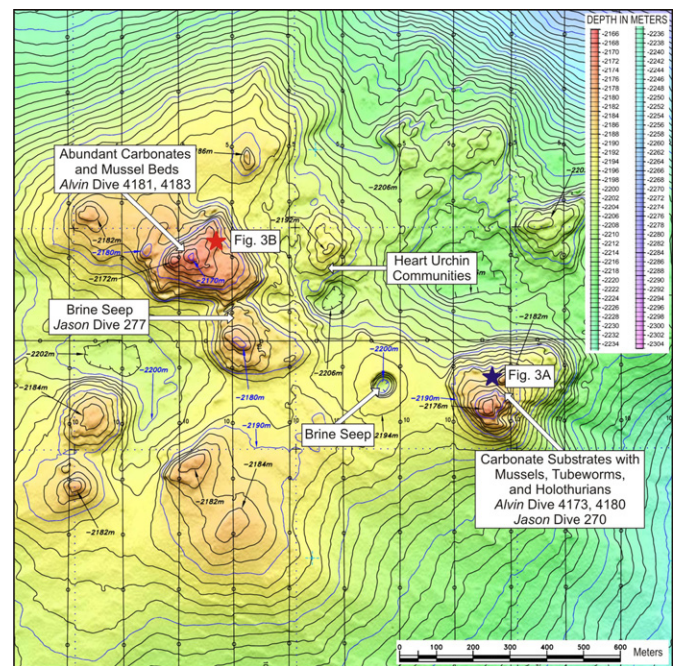


**Fig. 2.** A detailed multibeam bathymetry image acquired by the C-Surveyor II AUV over the AT340 site. The sample locations are marked with dive numbers. The positions of seafloor photographs in Fig. 3 are marked with two stars. Note the numerous local mounded features (expulsion sites) on top of an overall bathymetric high and the locations of features and our sample site (after Roberts et al., 2007b).
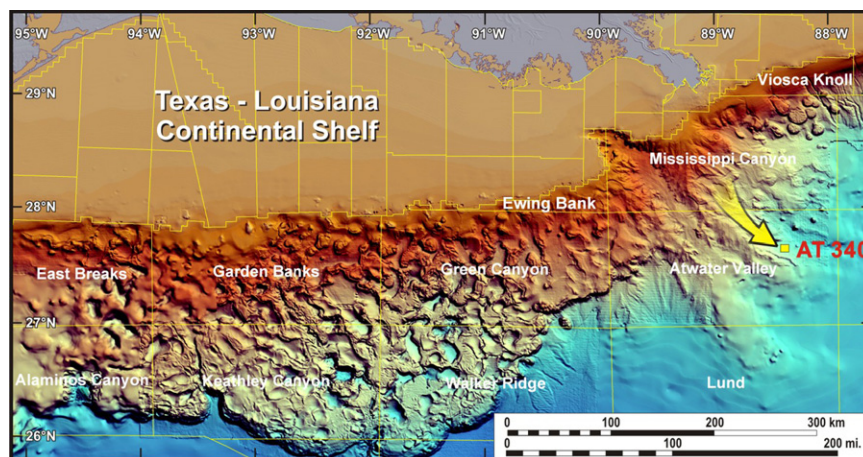


**Fig. 1.** A general overview of the seafloor morphology in the northern Gulf of Mexico. Atwater Valley lease area is identified and lease block 340 (AT340) is highlighted by a yellow arrow.
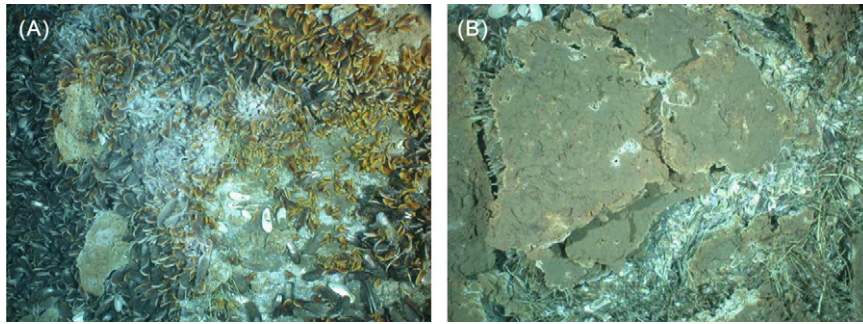
**Fig. 3.** Photographs acquired by DSV ALVIN. (A) This down-cam image shows two species of seep mussels in a dense bed at one of our sample sites. (B) Extensive carbonate pavements indicate protracted seepage. Fracturing and continuing colonization by mussels and tubeworms demonstrate ongoing seepage. Images are ~3 m across.

of mussel shells (Fig. 3B). Blocks of carbonate from this site had very little sediment matrix, only mussel shells and carbonate cements. Although most of the mussel shells did not house live mussels, several rather large areas of live mussels were observed at the three largest mounds of the AT340 site. Both the crest areas and flanks of the mound were covered with tubeworms. Many tubeworm colonies occurred beneath and at the edges of carbonate blocks, but free-standing colonies were also present. To the southeast and off the flank of the mound a brine seep was present (Fig. 2). Fluidized sediment, brine, and hydrocarbons were being seeped at this site. Mussel beds occurred around the seep site, and extensive mussel beds were found along the flow field.

The mussels at AT340 are primarily *Bathymodiolus brooksi*, and almost all of the tubeworms are *Escarpia laminata* (Erik E. Cordes, personal communication). Authigenic carbonate samples from mussel- and tubeworm-associated environments were collected using DSV ALVIN and ROV JASON from the subsurface of the seafloor. These samples were described, photographed, and subsequently stored at room temperature for sectioning, sub-sampling, and analysis.

# 3. Methods

## 3.1. Carbonate mineralogy and petrography

Bulk mineralogy and the relative abundance of carbonate minerals in each sample were determined by X-Ray Diffraction (XRD) using a Rigaku DXR 3000 computer-automated diffract-ometer at the Institute of Geochemistry, Chinese Academy of Sciences. Samples for XRD analyses were crushed into powder less than 300 mesh using a Micronizing Mill manufactured by McCrone Scientific Ltd. London, UK. The X-ray source was a Cu anode operated at 40 kV and 40 mA using CuKα radiation equipped with a diffracted beam graphite monochromator. The orientated samples were scanned at an interval of $5-65°$ (2θ) with a step size of $0.02°$ and count time of 5 seconds per step. Divergence, scattering, and receiving slits were $0.5°$, $0.5°$, and 0.15 mm, respectively. The relative proportions of different carbonate minerals were quantified on the basis of the (104) peak areas of calcite, Mg-calcite, and dolomite, and the (111) peak areas of aragonite using calibration curves (Greinert et al., 2001). The position of the (104) peak was used to determine the Mg content of carbonate minerals (Goldsmith et al., 1961; Lumsden, 1979). Calcite with less than 5 mol% $MgCO_3$ was considered low-Mg calcite (LMC) and calcite compositions of 5–20 mol% $MgCO_3$ were referred to as high-Mg calcite (HMC) (Burton and Walter, 1991). Carbonate phases with 30–40 mol% $MgCO_3$ were classified

as protodolomite, and carbonates containing 40–55 mol% $MgCO_3$ were referred to as dolomite (Naehr et al., 2007).

Petrographic observation of thin sections of the samples was made using an optical microscope. The microstructure of the seep carbonate on the fresh surfaces of broken samples was examined with a Scanning Electron Microscope (SEM). The samples were prepared by gold coating to a thickness of ~20 nm for the SEM observations. Photographs were taken using a JEOL 840 A SEM housed at the Department of Geology and Geophysics at Louisiana State University, operating at 10–20 kV with a 5–9 mm working distance.

## 3.2. Carbonate stable isotope analyses

Samples for oxygen and carbon analyses were obtained from the surfaces of polished slabs using a hand-held microdrill. Stable isotopes of carbon and oxygen were measured at the CAS Key Laboratory of Isotope Geochronology and Geochemistry, Guangz-hou Institute of Geochemistry, Chinese Academy of Sciences. The $CO_2$ extraction for analysis was obtained by reacting samples with 100% phosphoric acid at 90 °C. The purified $CO_2$ gas was analyzed using GV Isoprime II stable isotopic mass spectrometry. Results were reported in standard δ notation relative to the (Pee Dee Belemnite) PDB standard. Precision is on the order of 0.1‰ (2σ) for $δ^{13}C$ and 0.2‰ (2σ) for $δ^{18}O$.

# 4. Results

## 4.1. Occurrence of authigenic carbonates

Forty-five pieces of subsamples of the 12 samples associated with mussels and tubeworms were collected from the AT340 dive site. Six of the 12 representative samples are mussel-associated carbonates, and the other six are tubeworm-associated carbo-nates (Table 1). The majority of samples were obtained from blocks, slabs, crusts, and concretions (Fig. 4). Some of these are large samples, up to a half-meter long.

### 4.1.1. Mussel-associated carbonates

All carbonate samples were found on the surface of the seafloor. One big block, 15 cm in diameter and 45 cm long, collected from the large mussel bed during ALVIN dive 4180, is porous (cm-sized pores are common) and partly Fe/Mn coated (Fig. 4A). The cross section of this block exposes abundant cemented shell debris and carbonate cement. This cement, determined to be aragonite, occurs as void lining and isopachous rims (Fig. 4B). Irregular-shaped concretions of cm-sized were also

**Table 1**
Mineralogical composition of seep carbonates from mussel- and tubeworm-associated environments, AT340 of the Gulf of Mexico.

| Comments | Sample ID | Qtz (%) | LMC (%) | mol% Mg | HMC (%) | mol% Mg | Arag. (%) | Protodol./dolo. (%) | mol% Mg |
|---|---|---|---|---|---|---|---|---|---|
| Mussel grab | 4173-(1) | 8 | – | – | 73 | 8 | 27 | – | – |
| Mussel environment | 4180 | – | 7 | – | – | – | 93 | – | – |
| Mussel scoop | 4181 | 5 | – | – | 100 | 8 | – | – | – |
| Large mussel bed | 270-(44) | 3 | – | – | 23 | 14 | 77 | – | – |
| Grate mussel bed | 270-(57) | 2 | 3 | – | – | – | 97 | – | – |
| Mussel environment | 277-(12) | 5 | 23 | 1 | 5 | 13 | 72 | – | – |
| | | | | | | | | | |
| Tubeworm aggregation | 4173-(2) | 9 | 5 | – | – | – | 95 | – | – |
| Tubeworm (Bushmaster) | 4183-(1) | – | 4 | – | – | – | 96 | – | – |
| Baby tubeworms | 4183-(2) | 5 | – | – | 34 | 10 | 66 | – | – |
| Port Biobox tubeworm | 270-(43) | 4 | – | – | 48 | 13 | 52 | – | – |
| Below stained tubeworm | 270-(47) | 3 | – | – | 72 | 16 | 13 | 15 | 40 |
| Port Biobox tubeworm | 270-(52) | – | – | – | 54 | 13 | 39 | 7 | 30 |

Minerals: Qtz = quartz, LMC = low-Mg calcite, HMC = high-Mg calcite, Arag. = aragonite, Protodol./dolo. = protodolomite/dolomite.

## Mussel-associated carbonates



## Tubeworm-associated carbonates
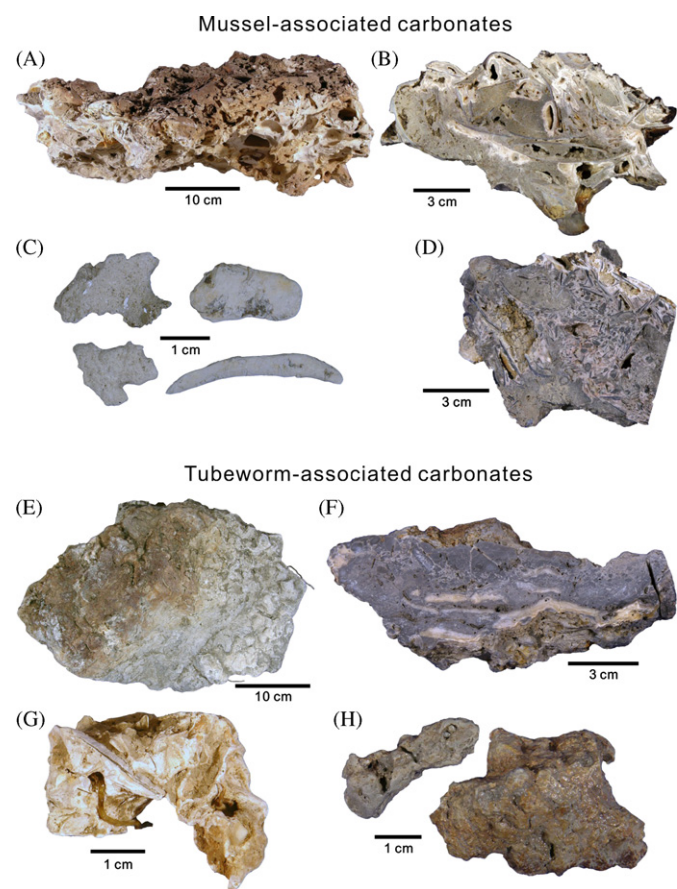
**Fig. 4.** Photographs of cold-seep carbonates derived from AT340. Carbonate collected from mussel-associated environments: (A) Massive carbonate, porous, and Fe/Mn coating (upper part). (B) A polished cut surface of the carbonate sample (A) showing abundant cemented shell debris. Aragonite occurs as void lining and isopachous rims. (C) Small carbonate samples of different shapes. (D) Highly brecciated matrix with abundant shell debris. Carbonate collected from tubeworm-associated environments: (E) Partly buried massive carbonate (the upper quarter is Fe/Mn coated). Note the posterior end of a tubeworm penetrating the carbonate at the lower right quarter. (F) Highly brecciated matrix with aragonite veins. (G) Irregular concretion collected from tubeworm environment with shell debris and tubeworm posterior end. (H) Carbonate concretions of different sizes below tubeworms.

obtained as independent samples (Fig. 4C). Fig. 4D illustrates a fragment from another large sample, up to 30 cm in diameter, collected from a brine seep during JASON dive 277 (sample location indicated in Fig. 2). It contains abundant shell debris and the matrix is highly brecciated.

### 4.1.2. Tubeworm-associated carbonates

Closer observations of tubeworm-associated carbonates indicate clear differences in overall macroscopic structure as compared to mussel-associated carbonates. One large sample, 25 cm in diameter and 35 cm long, collected during JASON dive 270, is massive, and its upper part is coated by Fe/Mn (Fig. 4E). The surface with limited Fe/Mn coating suggests that the sample has been buried beneath the water-sediment interface. The cross section of this block reveals that the matrix has been highly brecciated and carbonate cemented, with layered veins determined to be aragonite (Fig. 4F). Irregular concretions are common and usually are found beneath the sediment-water interface (Figs. 4G and 4H). The coexistence of live tubeworms and with shells suggests that tubeworms are younger than associated mussels (Fig. 4G). Accelerator Mass Spectrometry (AMS) radiocarbon dating reveals that the shell is about 10 ka old (unpublished data) and that the associated tubeworm was still alive during sample collection.

### 4.2. Mineralogy and petrology

#### 4.2.1. Mussel-associated carbonates

Mineralogy analyses of the matrix of carbonates from mussel-associated environments indicate that HMC and aragonite are the most abundant minerals, and that minor amounts of LMC and quartz occur (Table 1). The amounts of $MgCO_3$ in mussel-associated carbonates are relatively low; four of six samples range from 0 to 10 mol% and the other two range from 10 to 20 mol% (Fig. 5). The matrix is composed largely of peloids, foraminifers, shells, and shell fragments (Fig. 6A). Irregularly circular structure is also observed (Fig. 6B), suggesting multiple stages of cementations (Fig. 6B). Aragonite occurs both as microcrystalline cement and as banded, acicular crystals surrounding dark micritic peloids (Fig. 6C). The acicular aragonite cement sometimes originates from the surface of shells (Fig. 6D).

#### 4.2.2. Tubeworm-associated carbonates

Tubeworm-associated carbonates are also dominated by aragonite and HMC, with minor amounts of LMC and quartz, but a portion of dolomite was also identified in two samples (Table 1). The amounts of $MgCO_3$ in tubeworm-associated carbonates are relatively high; four of six samples range from 10 to 20 mol% and the other two range from 30 to 40 mol% (Fig. 5). Frequently, micritic HMC cements the pore space between individual sediment components, and sparitic aragonite fills voids and cracks between intraclasts (Fig. 7A). Layered aragonite
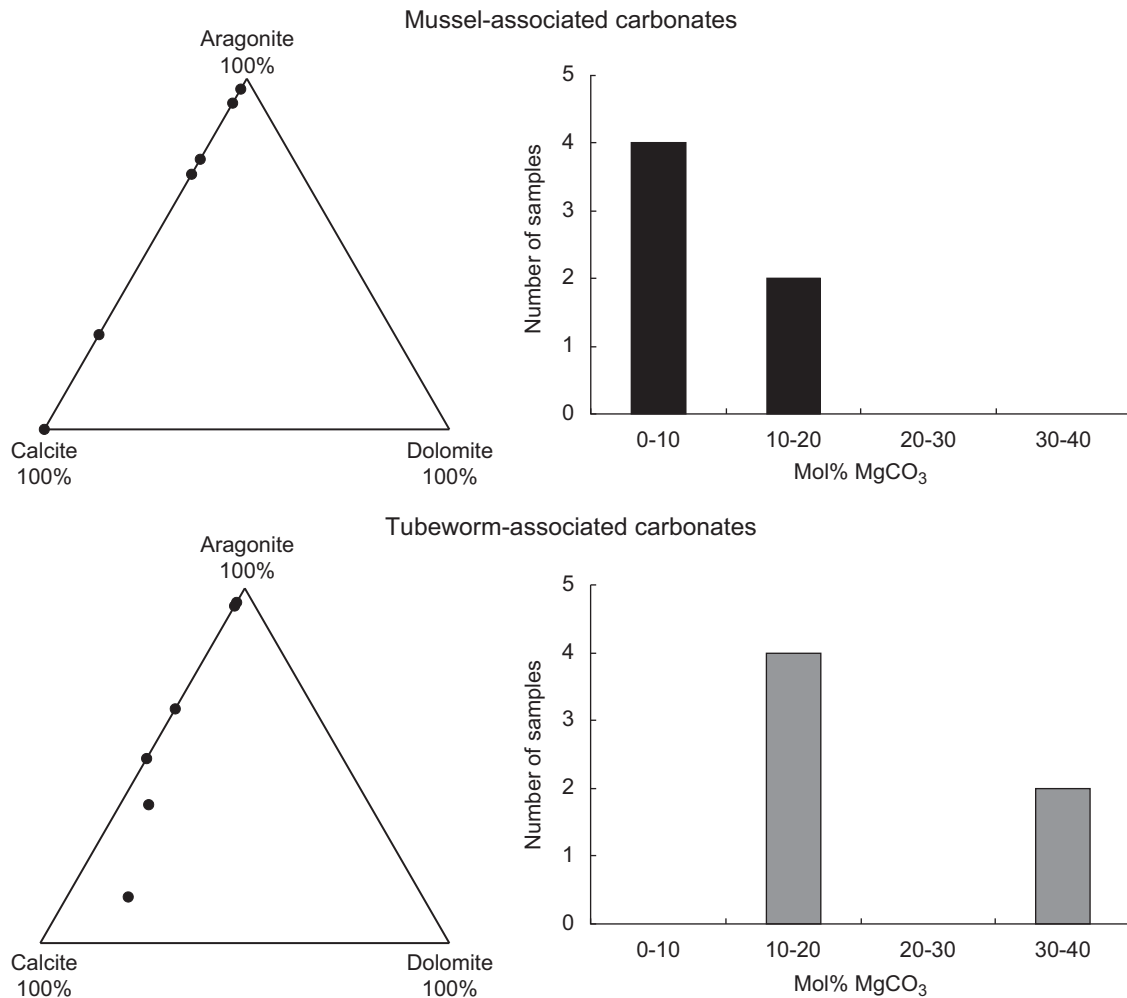
**Fig. 5.** Mineralogical composition of the carbonate fraction and frequency distribution of Mol% MgCO$_3$ in authigenic carbonates from mussel- and tubeworm-associated environments.

cement with multiple mineral growth is common (Fig. 7B). High-Mg calcite-cemented intercalates usually form a brecciated texture (Fig. 7C). Clotted micrites are common (Fig. 7D). Acicular aragonite cement fill large pore spaces (Fig. 8A), and distict crystals of micritic HMC (Fig. 8B) are common in both mussel- and tubeworm-associated carbonates. However, crystals with dolomite morphology but reduced Mg content (ratio of Ca/Mg > 2) are commonly observed in tubeworm-associated carbonates (Fig. 8C). These crystals frequently show a hole in their centers (Fig. 8D). A similar texture is described elsewhere and is proposed to represent a microbial origin (González et al., 2009).

### 4.3. Carbon and oxygen isotope data

#### 4.3.1. Carbon and oxygen isotope data of mussel-associated carbonates

The $\delta^{13}C$ values of mussel-associated carbonates vary between $-58.4$ and $-35.5‰$, but most data fall in the range of $-55$ to $-45‰$. The average $\delta^{13}C$ value of mussel-associated carbonate is $-51.8‰$ (n=61). Stable oxygen isotope compositions of the mussel-associated carbonates vary between 3.0 and 4.9‰ (average: 4.0‰, n=61; Fig. 9). No obvious difference occurs in $\delta^{13}C$ and $\delta^{18}O$ values between different carbonate facies, e.g., microcrystalline carbonate and botryoidal aragonite.

#### 4.3.2. Carbon and oxygen isotope data of tubeworm-associated carbonates

As in the case of mussel-associated carbonates, $\delta^{13}C$ values of tubeworm-associated carbonates are negative, ranging from $-60.8$ to $-47.7‰$. The average $\delta^{13}C$ value of tubeworm-associated carbonate is $-54.8‰$ (n=63). Stable oxygen isotope compositions of the mussel-associated carbonates vary between 3.1 and 5.1‰ (average: 4.0‰, n=63; Fig. 9). The range and average $\delta^{18}O$ data are rather consistent between mussel- and tubeworm-associated carbonates. Like mussel-associated carbonates, there is only a small variation between different carbonate facies (microcrystalline carbonate and botryoidal aragonite) for tubeworm-associated carbonates in both $\delta^{13}C$ and $\delta^{18}O$ values.

### 5. Discussion

#### 5.1. Mineral composition of mussel- and tubeworm-associated carbonates

Unlike the hydrocarbon-derived carbonates described by Feng et al. (2008; 2009) from Alaminos Canyon block 645 (AC645) and Bush Hill (GC185), which are dominated by aragonite mineralogy, authigenic carbonates produced by similar processes at AT340 on the continental slope of the northern Gulf of Mexico show a greater mineralogical complexity (Table 1). However, a wide
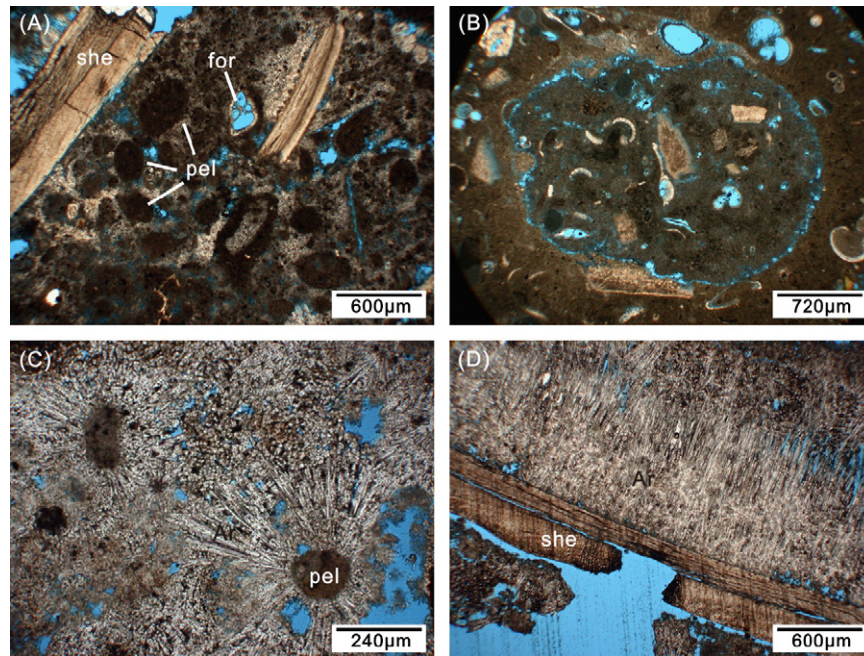
**Fig. 6.** Photomicrographs of representative seep carbonate samples from mussel-associated environments: (A) Matrix has peloid (labeled "pel"), foraminifer (labeled "for"), and shell (labeled "she"), plane polarized light. (B) Matrix has an irregularly circular structure, suggesting multiple stages of cementations, plane polarized light. (C) Circumgranular aragonite cement around dark, micritic peloids, plane polarized light. (D) Acicular aragonites originate from shells, plane polarized light.
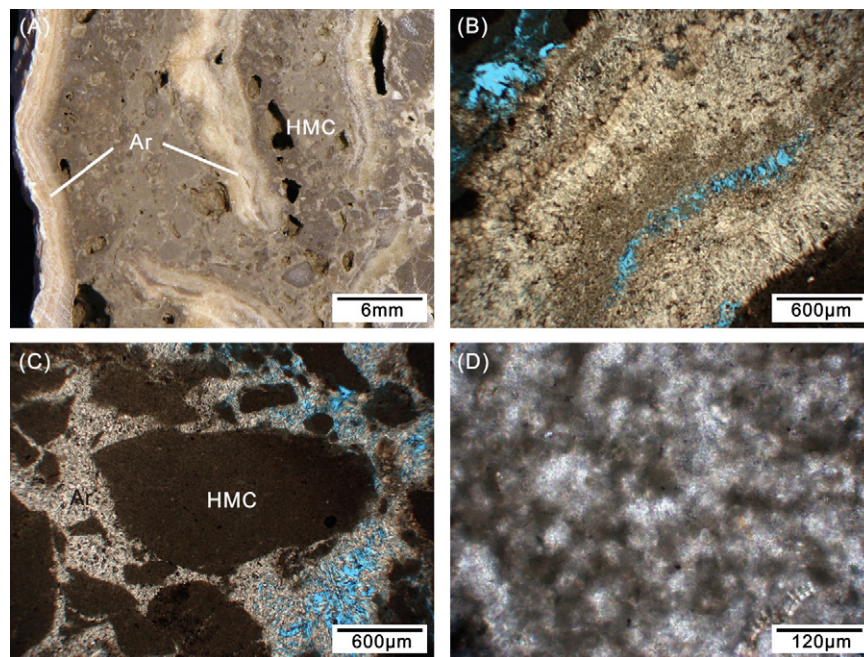


**Fig. 7.** Hand specimen and photomicrographs of cold-seep carbonates from tubeworm-associated environments: (A) textural relationship between HMC (dark gray) and aragonite (white) in hand specimen. (B) Detailed view of aragonite in (A) showing multiple mineral growth, plane polarized light. (C) HMC-cemented intercalates (dark) forming a brecciated texture, plane polarized light. (D) Clotted micrites are common, which usually show indistinct boundaries and with aragonite cement filling the pore space between the clots, plane polarized light.

range of mineralogical variation in authigenic carbonates within individual study areas but common trend across multiple geographic areas has been suggested by the study of samples from whole continental slope of the Gulf of Mexico (Roberts and Aharon, 1994; Roberts et al., 2010).

Authigenic carbonate precipitation at hydrocarbon seep sites will take place only when pore fluids become sufficiently supersaturated with respect to a carbonate phase and crystallization is not inhibited by kinetic factors (Burton, 1993). Factors that influence carbonate mineral precipitation at hydrocarbon seep sites include the degree of carbonate super-saturation, the concentrations of Ca and Mg, the presence of complex-forming anions such as $SO_4^{2-}$ and $PO_4^{3-}$, temperature, $pCO_2$, the degree of microbial activity, and the phylogeny of the microbes involved (Naehr et al., 2007 and references therein). Previous studies suggest that in general aragonite seems to be
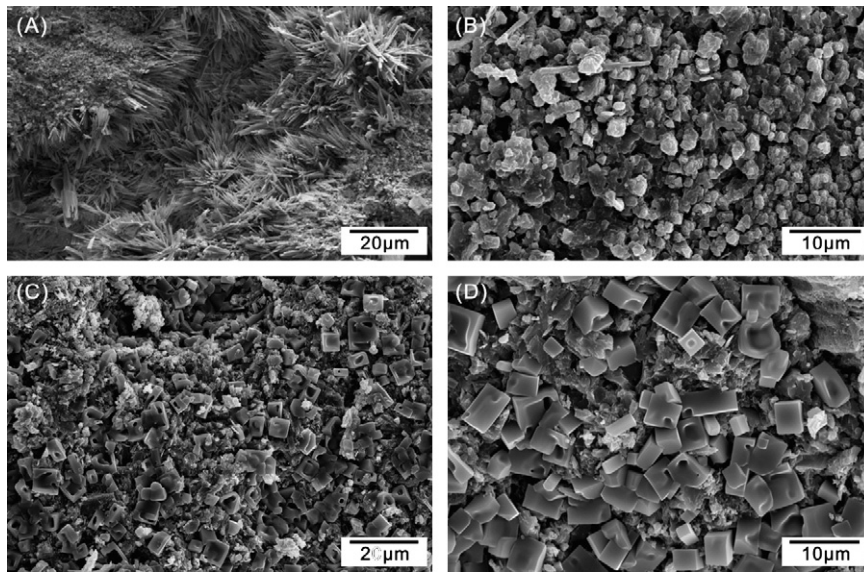
**Fig. 8.** Scanning electron microscopy photographs of seep carbonates. (A) Microcrystalline aragonite and pore-filling acicular aragonite in mussel-associated carbonate. (B) HMC grains in mussel-associated carbonate. (C) Dolomite crystals in tubeworm-associated carbonate. (D) Detail of dolomite crystals in (C).
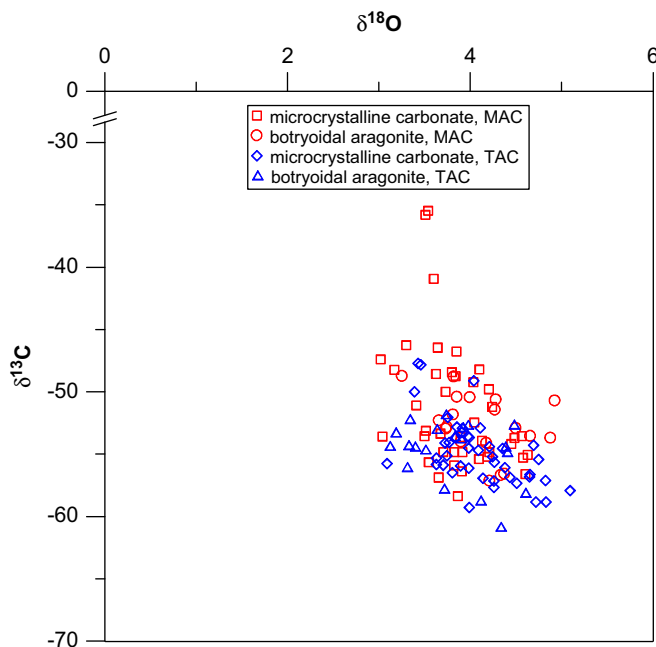


**Fig. 9.** Plot of $\delta^{13}C$ and $\delta^{18}O$ values of seep carbonates from mussel- and tubeworm-associated environments. MAC=mussel-associated carbonates, TAC=tubeworm-associated carbonates.



**Fig. 10.** Histogram illustrating the frequency distribution of $\delta^{13}C$ values of seep carbonates from mussel- and tubeworm-associated environments. MAC=mussel-associated carbonates, TAC=tubeworm-associated carbonates. The $\delta^{13}C$ of mussel-associated carbonates is generally higher than that of tubeworm-associated carbonates.

favored in high $SO_4^{2-}$ environments with higher total alkalinity concentrations (Burton, 1993; Savard et al., 1996). The crystallization of Mg-calcite preferentially occurs under conditions with lower $SO_4^{2-}$ and total alkalinity concentrations (Greinert et al., 2001). The mechanism for formation of dolomite at hydrocarbon seeps is still poorly understood. However, this dolomite is clearly of microbial origin and is related to the methanotrophic prokaryotes, either methanotrophic archaea or methanotrophic bacteria (Peckmann et al., 1999; Peckmann and Thiel, 2004).

Results of XRD analysis illustrated that carbonates from tubeworm-associated environments have relatively higher amounts of $MgCO_3$ than mussel-associated carbonates (Fig. 5). High-Mg calcite commonly contains $MgCO_3 < 20\%$, whereas extreme HMC (amount of $MgCO_3 > 20$ mol%) is rarely reported

in the literature (e.g., Ferrell and Aharon, 1994; Han et al., 2008). However, the formation mechanism of HMC and its relationship with dolomite remain unclear. Ferrell and Aharon (1994) suggested that the role of the seep microenvironment is most important in determining the Mg content of the magnesium calcites at seep sites. Han et al. (2008) reported that extreme HMC may eventually transform into dolomites.

The AT340 seep carbonate samples may provide further insight into the formation of dolomite at hydrocarbon seep environments. Although additional geochemical data (e.g., biomarkers) are needed for further investigation, we currently propose that microbial activity, most probably by consortia of Anaerobic

Methane-Oxidizing Archaea (ANME) and Sulfate Reducing Bacteria (SRB) at seep sites play an important role in formation of dolomite. In this study, dolomite occurs only in samples from tubeworm-associated environments (Table 1 and Fig. 5). The precipitation of dolomite has been observed in seep carbonates extensively (e.g., Roberts and Aharon, 1994; Peckmann et al., 1999; Moore et al., 2004; Peckmann and Thiel, 2004; Takeuchi et al., 2007), and dolomite precipitation was interpreted to be related to bacterial activity (Peckmann et al., 1999; Peckmann and Thiel, 2004; Takeuchi et al., 2007). Tubeworms are dependent on symbiotic sulfide-oxidizers, and may be able to stimulate SRB activity in the sediment by sulfate pumping (cf. Cordes et al., 2005; Dattagupta et al., 2006, 2008). Mediation of SRB as a possible mechanism for natural and culture experiments of the formation of dolomite at low temperatures has been reported previously (e.g., Vasconcelos et al., 1995; Vasconcelos and McKenzie, 2000). Thus, it is suggested that there may be a potential relationship between the activity of SRB and dolomite precipitation at hydrocarbon seeps.

## 5.2. Carbon sources of seep carbonates and depleted $^{13}C$ of tubeworm-associated carbonates

In the Gulf of Mexico, $\delta^{13}C$ values of seep-related carbonates vary from roughly $-60‰$ to $14‰$ (Roberts and Aharon, 1994; Chen et al., 2007; Feng et al., 2008; 2009; Roberts et al., 2010). Large variation of stable isotopic composition in authigenic carbonates occurs both within individual study areas (e.g., over 40‰ at AC601) and across multiple geographic areas (Roberts et al., 2010), although the latter is more likely.

The carbonate carbon isotope values (from $-60.8‰$ to $-35.5‰$; Fig. 9) of this study are lower than those found in any known carbon source other than methane. The $\delta^{13}C$ values of microbial methane are typically $< -60‰$, whereas thermogenic methane of $\delta^{13}C$ values are typically $> -50‰$ (Bernard et al., 1978). In addition, parent methane is usually significantly more depleted in $^{13}C$ than the resulting carbonate precipitates (Peckmann and Thiel, 2004; Roberts et al., 2010). Thus, the carbon source for the authigenic carbonate in this study is derived mainly from $^{13}C$-depleted biogenic methane. In the GOM, cold-seep carbonate with such low carbon isotope values ($< -60‰$) has been reported only from Tunica Mound (GB386) and Mississippi Canyon (Chen et al., 2007).

Authigenic carbonate samples from tubeworm-associated environments yielded more negative $\delta^{13}C$ values (average: $-53.8‰$, $n=63$) than the authigenic carbonate samples from mussel-associated environments (average: $-51.8‰$, $n=61$; Fig. 10), this difference is not a function of mineralogy because the mineral composition of the carbonates from both mussel- and tubeworm-associated environments is similar, as both are dominated by HMC and aragonite (Table 1 and Fig. 5).

The possible mechanisms for the relatively lower $\delta^{13}C$ values of tubeworm-associated carbonates are (1) carbon isotopic vital effect of seep animals, (2) fluid physical pumping of mussels, and (3) release of sulfate by tubeworms through their roots. The $\delta^{13}C$ values of the tissues of mussels are generally lower than those of tubeworms at AT340 seep sites (Becker et al., 2010 and unpublished data). Mussels are preferentially taking up $^{13}C$-depleted methane and fixing the carbon into their tissues, resulting in local $^{13}C$ enrichment in the surrounding sediments; this information is finally recorded in the associated carbonates. An alternate possibility could be the physical action of mussels moving seawater around and increasing the amount of seawater $CO_2$ in the dissolved inorganic carbon (DIC) pool around the mussel bed. Finally, some genera of tubeworms (e.g., Lamellibrachia) appear to release sulfate through

their roots, increasing the sulfate-reducing rate (Cordes et al., 2005; Dattagupta et al., 2008). At hydrocarbon seep sites, the oxidation of the ascending methane is coupled with sulfate reduction near the sediment surface, where sulfide and bicarbonate are released (Boetius et al., 2000):

$$CH_4 + SO_4^{2-} \rightarrow HCO_3^- + HS^- + H_2O \qquad (1)$$

Microbial sulfate reduction in organic-rich sediments can be limited by sulfate availability, and tubeworms could theoretically enhance sulfate reduction near their roots by supplying sulfate across their root surface into the surrounding sediment (Cordes et al., 2005; Dattagupta et al., 2006, 2008). The carbon isotope shift from $CH_4$ to $HCO_3^-$, caused by isotopic fractionation during AOM, can be as large as $-10‰$ (Alperin and Reeburgh, 1988; Martens et al., 1999; Formolo et al., 2004). Increase of sulfate reduction and coupled methane oxidation rates can therefore increase the supply of $^{13}C$-depleted carbonate ions, which results in lower $\delta^{13}C_{carbonate}$ values. Although Escarpia is more closely related to Seepiophila than to Lamellibrachia, Seepiophila does not appear to rely on its roots to release sulfate. The relationship with tubeworm root function does not eliminate this pathway as a possibility, but makes it a little less likely (Erik E. Cordes, personal communication). Thus, we hypothesize that the physiology of mussels and tubeworms results in more negative $\delta^{13}C$ values of tubeworm-associated carbonates compared to the mussel-associated carbonates at hydrocarbon seeps.

## 5.3. Conceptual model for the evolution of seep macrofauna

Authigenic carbonates are typically associated with mussels and tubeworms at hydrocarbon seeps. These carbonates also serve as substrates for many other marine organisms (e.g., Fisher et al., 1997; Bergquist et al., 2002; Jørgensen and Boetius, 2007). Seep-related carbonates are found in areas of prolonged and active hydrocarbon seeps (e.g., Roberts and Aharon, 1994; Sassen et al., 1994; Peckmann and Thiel, 2004). Mussels and tubeworms exhibit longevity that ranges over a few centuries when methane and sulfide are available at the subsurface seafloor (e.g., Bergquist et al., 2002; Cordes et al., 2003). However, fluid-gas migration of hydrocarbons to the seafloor can vary over short time periods at seepage sites occupied by mussel and tubeworm aggregations (Tryon and Brown, 2004; Levin, 2005; Solomon et al., 2008).

Fig. 11 is a schematic diagram for the evolution of seep macrofauna of a cold-seep system at AT340 of the GOM. The environment is dominated by a rather abundant and constant supply of methane, resulting in a methane-dominated chemosynthesis-based community of mostly mussels. Sulfate-Hydrocarbon Transition (SHT) lies at relatively shallow depth (Fig. 11A). The flux of methane controls the thickness of the zone of sulfate reduction. Carbonates precipitated at this stage usually occur at the surface or in the very shallow subsurface. As the seepage occurs, the AOM (Eq. 1) releases sulfide hydrogen and bicarbonate. A sulfide-dominated chemosynthesis-based community, mostly tubeworms, begins to flourish, and the seep system changes to a mixed mussel-tubeworm environment (Fig. 11B). At the same time, the precipitation of carbonate continues and may restrict the gas flux. However, carbonate precipitation may also increase methane flux locally by channelling flow into an increasingly small number of cracks and conduits, which is the reason macrofauna are usually restricted to the periphery of carbonate slabs (Fig. 3). A third stage occurs if the flux of methane slows dramatically. The seep site is dominated by a steady supply of hydrogen sulfide, which is produced by sulfate reduction using the sediment-trapped methane, resulting in a tubeworm-dominated environment
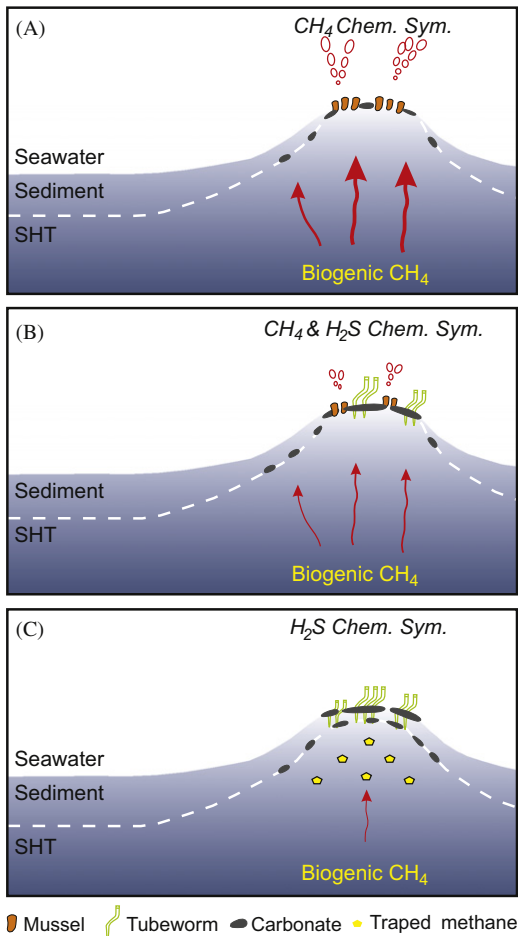
**Fig. 11.** Schematic diagram of seep carbonate precipitation from mussel- and tubeworm-associated environments. Model illustrates the evolution from mussel-dominated to tubeworm-dominated habitat. SHT, sulfate hydrocarbon transition.

(Fig. 11C). The sulfate-hydrocarbon transition migrates downward. Carbonates precipitated at this stage usually occur slightly deeper, below the sediment-water interface.

As we have discussed, similar distributions of seep macrofauna have been reported from ancient hydrocarbon seep regions of New Zealand and Japan, where the mussel beds are commonly overlain by thickets of calcareous tubes (cf. Campbell et al., 2002, 2008; Jenkins et al., 2007). The evolution of seep macrofauna addressed in this study is controlled mainly by change of seep habitat, e.g., the seep flux change rather than the true ecological succession. In this study (on ALVIN dive 4173), cores were collected near tubeworm bushes and from a mussel bed. Methane concentrations in the pore water near the tubeworm bush were low ($< 20\,\mu M$), whereas concentrations near the mussel bed were extremely high, up to 3 mM (CHEMO III cruise report, 2007), a finding that is consistent with the fact that methane concentrations are correlated with seepage rates at seeps (Torres et al., 2002).

## 6. Conclusions

Petrographic and geochemical analyses of authigenic carbonates from mussel- and tubeworm-associated environments from hydrocarbon seeps at AT340 of the GOM reveal differences in both mineralogy and stable carbon isotopes. Both mussel- and tubeworm-associated carbonates are dominated by HMC and aragonite. With respect to HMC, the tubeworm-associated carbonate

samples have relatively higher amounts of $MgCO_3$, and even dolomite, as reflected by $30-40$ mol% $MgCO_3$ when compared to mussel-associated carbonates. Low $\delta^{13}C_{carbonate}$ values (as low as $-60.8‰$) indicate that the carbon source was mainly methane. The $\delta^{13}C$ values of tubeworm-associated carbonates are generally more negative than those of mussel-associated carbonates. The possible mechanisms responsible for this phenomenon are: (1) mussels are preferentially taking up $^{13}C$-depleted methane and fixing the carbon into their tissues, resulting in locally $^{13}C$ enrichment in the surrounding sediments, (2) physical action of mussels moving seawater around and increasing the amount of seawater carbonate ions in the dissolved inorganic carbon (DIC) pool around the mussel bed; and (3) tubeworms may release sulfate through their roots, increasing sulfate-reducing and coupled anaerobic oxidation of methane rates, which increases the supply of $^{13}C$-depleted carbonate ions and finally results in lower $d^{13}C_{carbonate}$ values.

The heterogeneities in isotopic and mineralogical variation in authigenic carbonate composition within mussel- and tubeworm-associated carbonates probably reflect local controls of temporal evolution of hydrocarbon seeps and associated seep macrofaunas, particularly seep mussels and tubeworms. We presume that the geochemical evolution of seep macrofauna is usually from a mussel-dominated environment to a mixed mussel-tubeworm environment, and eventually to a mostly tubeworm-dominated environment. Finally, the responses of the evolution of the seep macrofauna to the cold-seep carbonates geology and geochemistry discussed in this paper are end-member types. However, because of the episodic nature of expulsion events and systematic changes in the flux at a given site, the types of seafloor may shift from one part of the response spectrum to another, given sufficient time. Our study is an initial effort to determine whether the authigenic carbonates of mussel and tubeworm environments are different and whether these differences can be used as a way to distinguish ancient seep carbonates from these two settings.

## References

Alperin, M.J., Reeburgh, W.S., 1988. Carbon and hydrogen isotope fractionation resulting from anaerobic methane oxidation. Global Biogeochemical Cycles 2 (3), 279–288.
Becker, E.L., Raymond, W.L., Stephen, A.M., Fisher, C.R., 2010. Stable carbon and nitrogen isotope composition of hydrocarbon seep bivalves on the lower continental slope of the Gulf of Mexico. Deep-Sea Research II 57 (21–23), 1957–1964.

Bergquist, D.C., Urcuyo, I.A., Fisher, C.R., 2002. Establishment and persistence of seep vestimentiferan aggregations on the upper Louisiana slope of the Gulf of Mexico. Marine Ecology - Progress Series 241, 89–98.

Bernard, B.B., Brooks, J.M., Sackett, W.M., 1978. Light-hydrocarbons in recent Texas continental-shelf and slope sediments. Journal of Geophysical Research - Oceans and Atmospheres 83 (NC8), 4053–4061.

Boetius, A., Ravenschlag, K., Schubert, C.J., Rickert, D., Widdel, F., Gieseke, A., Amann, R., Jorgensen, B.B., Witte, U., Pfannkuche, O., 2000. A marine microbial consortium apparently mediating anaerobic oxidation of methane. Nature 407 (6804), 623–626.

Burton, E.A., 1993. Controls on marine carbonate cement mineralogy: review and reassessment. Chemical Geology 105 (1–3), 163–179.

Burton, E.A., Walter, L.M., 1991. The effects of $P_{CO2}$ and temperature on magnesium incorporation in calcite in seawater and $MgCl_2$-$CaCl_2$ solutions. Geochimica et Cosmochimica Acta 55 (3), 777–785.

CHEMO III Cruise Report 2007. Deep chemosynthetic community characterization cruise report. ⟨http://www.tdi-bi.com/chemo3/Cruise3_607/DCR2_CruRpt_Sep27.pdf⟩.

Campbell, K.A., 2006. Hydrocarbon seep and hydrothermal vent paleoenvironments and paleontology: Past developments and future research directions. Palaeogeography, Palaeoclimatology, Palaeoecology 232 (2–4), 362–407.

Campbell, K.A., Farmer, J.D., Des Marais, D., 2002. Ancient hydrocarbon seeps from the Mesozoic convergent margin of California: carbonate geochemistry, fluids and palaeoenvironments. Geofluids 2 (2), 63–94.

Campbell, K.A., Francis, D.A., Collins, M., Gregory, M.R., Nelson, C.S., Greinert, J., Aharon, P., 2008. Hydrocarbon seep-carbonates of a Miocene forearc (East Coast Basin), North Island, New Zealand. Sedimentary Geology 204 (3–4), 83–105.

Chen, Y., Matsumoto, R., Paull, C.K., Ussler III, W., Lorenson, T., Hart, P., Winters, W., 2007. Methane-derived authigenic carbonates from the northern Gulf of Mexico - MD02 Cruise. Journal of Geochemical Exploration 95 (1–3), 1–15.

Cordes, E.E., Arthur, M.A., Shea, K., Arvidson, R.S., Fisher, C.R., 2005. Modeling the mutualistic interactions between tubeworms and microbial consortia. Plos Biology 3 (3), 497–506.

Cordes, E.E., Bergquist, D.C., Shea, K., Fisher, C.R., 2003. Hydrogen sulphide demand of long-lived vestimentiferan tubeworm aggregations modifies the chemical environment at deep-sea hydrocarbon seeps. Ecology Letters 6 (3), 212–219.

Cordes, E.E., Bergquist, D.C., Fisher, C.R., 2009. Macro-ecology of Gulf of Mexico cold seeps. Annual Review of Marine Science 1 (1), 143–168.

Dattagupta, S., Arthur, M.A., Fisher, C.R., 2008. Modification of sediment geochemistry by the hydrocarbon seep tubeworm *Lamellibrachia luymesi*: A combined empirical and modeling approach. Geochimica et Cosmochimica Acta 72 (9), 2298–2315.

Dattagupta, S., Miles, L.L., Barnabei, M.S., Fisher, C.R., 2006. The hydrocarbon seep tubeworm *Lamellibrachia luymesi* primarily eliminates sulfate and hydrogen ions across its roots to conserve energy and ensure sulfide supply. Journal of Experimental Biology 209 (19), 3795–3805.

Feng, D., Chen, D.F., Qi, L., Roberts, H.H., 2008. Petrographic and geochemical characterization of seep carbonate from Alaminos Canyon, Gulf of Mexico. Chinese Science Bulletin 53 (11), 1716–1724.

Feng, D., Chen, D.F., Roberts, H.H., 2009. Petrographic and geochemical characterization of seep carbonate from Bush Hill (GC185) gas vent and hydrate site of the Gulf of Mexico. Marine and Petroleum Geology 26 (7), 1190–1198.

Ferrell, R.E., Aharon, P., 1994. Mineral assemblages occurring around hydrocarbon vents in the northern Gulf of Mexico. Geo-Marine Letters 14 (2–3), 74–80.

Fisher, C.R., Urcuyo, I.A., Simpkins, M.A., Nix, E., 1997. Life in the slow lane: growth and longevity of cold-seep vestimentiferans. Marine Ecology 18 (1), 83–94.

Formolo, M.J., Lyons, T.W., Zhang, C., Kelley, C., Sassen, R., Horita, J., Cole, D.R., 2004. Quantifying carbon sources in the formation of authigenic carbonates at gas hydrate sites in the Gulf of Mexico. Chemical Geology 205 (3–4), 253–264.

Goldsmith, J.R., Graf, D.L., Heard, H.C., 1961. Lattice constants of the calcium-magnesium carbonates. American Mineralogist 46 (3–4), 453–457.

González, F.J., Somoza, L., Lunar, R., Martínez-Frías, J., Martín Rubí, J.A., Torres, T., Ortiz, J.E., Díaz del Río, V., Pinheiro, L.M., Magalhães, V.H., 2009. Hydrocarbon-derived ferromanganese nodules in carbonate-mud mounds from the Gulf of Cadiz: Mud-breccia sediments and clasts as nucleation sites. Marine Geology 261 (1–4), 64–81.

Greinert, J., Bohrmann, G., Suess, E., 2001. Gas hydrate associated carbonates and methane-venting at Hydrate Ridge: classification, distribution and origin of authigenic lithologies. In: Paull, C.K., Dillon, W.P. (Eds.), Natural Gas Hydrates: Occurrence, Distribution, and Detection. American Geophysical Union, Washington, DC, USA, pp. 91–113.

Han, X., Suess, E., Huang, Y., Wu, N., Bohrmann, G., Su, X., Eisenhauer, A., Rehder, G., Fang, Y., 2008. Jiulong methane reef: Microbial mediation of seep carbonates in the South China Sea. Marine Geology 249 (3–4), 243–256.

Hinrichs, K.U., Hayes, J.M., Sylva, S.P., Brewer, P.G., DeLong, E.F., 1999. Methane-consuming archaebacteria in marine sediments. Nature 398 (6730), 802–805.

Jenkins, R.G., Kaim, A., Hikida, Y., Tanabe, K., 2007. Methane-flux-dependent lateral faunal changes in a Late Cretaceous chemosymbiotic assemblage from the Nakagawa area of Hokkaido. Japan. Geobiology 5 (2), 127–139.

Jørgensen, B.B., Boetius, A., 2007. Feast and famine - microbial life in the deep-sea bed. Nature Reviews Microbiology 5 (10), 770–781.

Joye, S.B., Boetius, A., Orcutt, B.N., Montoya, J.P., Schulz, H.N., Erickson, M.J., Lugo, S.K., 2004. The anaerobic oxidation of methane and sulfate reduction

in sediments from Gulf of Mexico cold seeps. Chemical Geology 205 (3–4), 219–238.

Lessard-Pilon, S.A., Podowski, E.L., Cordes, E.E., Fisher, C.R., 2010. Community composition and temporal change at deep Gulf of Mexico cold seeps. Deep-Sea Research II 57 (21–23), 1891–1903.

Levin, L.A., 2005. Ecology of cold seep sediments: Interactions of fauna with flow, chemistry and microbes. Oceanography and Marine Biology - an Annual Review, 43. CRC Press-Taylor & Francis Group, Boca Raton, FL, USA 1–46.

Luff, R., Wallmann, K., 2003. Fluid flow, methane fluxes, carbonate precipitation and biogeochemical turnover in gas hydrate-bearing sediments at Hydrate Ridge, Cascadia Margin: numerical modeling and mass balances. Geochimica et Cosmochimica Acta 67 (18), 3403–3421.

Lumsden, D.N., 1979. Error in X-ray diffraction estimates of dolomite in carbonate rocks—causes and cures. American Association of Petroleum Geologists Bulletin 63 (3), 488.

Martens, C.S., Albert, D.B., Alperin, M.J., 1999. Stable isotope tracing of anaerobic methane oxidation in the gassy sediments of Eckernforde Bay. German Baltic Sea. American Journal of Science 299 (7–9), 589–610.

Moore, T.S., Murray, R.W., Kurtz, A.C., Schrag, D.P., 2004. Anaerobic methane oxidation and the formation of dolomite. Earth and Planetary Science Letters 229 (1–2), 141–154.

Naehr, T.H., Eichhubl, P., Orphan, V.J., Hovland, M., Paull, C.K., Ussler III, W., Lorenson, T.D., Greene, H.G., 2007. Authigenic carbonate formation at hydrocarbon seeps in continental margin sediments: A comparative study. Deep-Sea Research II: Topical Studies in Oceanography 54 (11–13), 1268–1291.

Peckmann, J., Thiel, V., Michaelis, W., Clari, P., Gaillard, C., Martire, L., Reitner, J., 1999. Cold seep deposits of Beauvoisin (Oxfordian; southeastern France) and Marmorito (Miocene; northern Italy): microbially induced authigenic carbonates. International Journal of Earth Sciences 88 (1), 60–75.

Peckmann, J., Thiel, V., 2004. Carbon cycling at ancient methane-seeps. Chemical Geology 205 (3–4), 443–467.

Roberts, H.H., Aharon, P., 1994. hydrocarbon-derived carbonate buildups of the northern Gulf of Mexico continental slope - a review of submersible investigations. Geo-Marine Letters 14 (2–3), 135–148.

Roberts, H.H., Aharon, P., Carney, R., Larkin, J., Sassen, R., 1990. Sea-floor responses to hydrocarbon seeps, Louisiana continental slope. Geo-Marine Letters 10 (4), 232–243.

Roberts, H.H., Carney, R.S., 1997. Evidence of episodic fluid, gas, and sediment venting on the northern Gulf of Mexico continental slope. Economic Geology and the Bulletin of the Society of Economic Geologists 92 (7–8), 863–879.

Roberts, H., 2001. Fluid and gas expulsion on the northern Gulf of Mexico continental slope: mud-prone to mineral-prone responses. In: Paull, C.K., Dillon, W.P. (Eds.), Natural Gas Hydrates: Occurrence, Distribution, and Detection. American Geophysical Union, Washington, DC, USA, pp. 145–161.

Roberts, H.H., Fisher, C., Bernard, B., Brooks, J., Bright, M., Carney, R., Cordes, E., Hourdez, S., Hunt, J., Joye, S., MacDonald, I., Morrison, C., Nelson, K., Samarkin, V., Shedd, W., Becker, E., Bernier, M., Bowles, M., Goehring, L., Kupehik, M., Lessard-Pilon, S., Niemann, H., Petersen, C., Petersen, J., Potter, J., Telesnicki, G., 2007a. ALVIN explores the deep northern Gulf of Mexico slope. EOS Transactions of the American Geophysical Union 88, 341–342.

Roberts, H.H., Fisher, C.R., Brooks, J.M., Bernard, B., Carney, R.S., Cordes, E., Shedd, W., Hunt, J., Joye Jr., S., MacDonald, I.R., Morrison, C., 2007b. Exploration of the deep Gulf of Mexico slope using DSV Alvin: Site selection and geologic character. Gulf Coast Association of Geological Societies Transactions 57, 647–659.

Roberts, H., Feng, D., Joye, S.B., 2010. Cold seep carbonates of the middle and lower continental slope, northern Gulf of Mexico. Deep-Sea Research II 57 (21–23), 2040–2054.

Sassen, R., Macdonald, I.R., Requejo, A.G., Guinasso, N.L., Kennicutt, M.C., Sweet, S.T., Brooks, J.M., 1994. Organic geochemistry of sediments from chemosynthetic communities, Gulf-of-Mexico slope. Geo-Marine Letters 14 (2–3), 110–119.

Savard, M.M., Beauchamp, B., Veizer, J., 1996. Significance of aragonite cements around Cretaceous marine methane seeps. Journal of Sedimentary Research 66 (3), 430–438.

Solomon, E.A., Kastner, M., Jannasch, H., Robertson, G., Weinstein, Y., 2008. Dynamic fluid flow and chemical fluxes associated with a seafloor gas hydrate deposit on the northern Gulf of Mexico slope. Earth and Planetary Science Letters 270 (1–2), 95–105.

Takeuchi, R., Matsumoto, R., Ogihara, S., Machiyama, H., 2007. Methane-induced dolomite "chimneys" on the Kuroshima Knoll, Ryukyu islands, Japan. Journal of Geochemical Exploration 95 (1–3), 16–28.

Tryon, M.D., Brown, K.M., 2004. Fluid and chemical cycling at Bush Hill: implications for gas- and hydrate-rich environments. Geochemistry, Geophysics, Geosystems 5 (12), Q12004, doi:10.1029/2004GC000778.

Torres, M.E., McManus, J., Hammond, D.E., de Angelis, M.A., Heeschen, K.U., Colbert, S.L., Tryon, M.D., Brown, K.M., Suess, E., 2002. Fluid and chemical fluxes in and out of sediments hosting methane hydrate deposits on Hydrate Ridge, OR, I: Hydrological provinces. Earth and Planetary Science Letters 201 (3–4), 525–540.

Vasconcelos, C., McKenzie, J.A., 2000. Biogeochemistry - sulfate reducers - dominant players in a low-oxygen world? Science 290 (5497) 1711–1712.

Vasconcelos, C., McKenzie, J.A., Bernasconi, S., Grujic, D., Tien, A.J., 1995. Microbial mediation as a possible mechanism for natural dolomite formation at low-temperatures. Nature 377 (6546), 220–222.